JGR Oceans

RESEARCH ARTICLE
10.1029/2019JC015534

Special Section:
Years of the Maritime Continent

Advection by the North Equatorial Current of a Cold Wake due to Multiple Typhoons in the Western Pacific: Measurements From a Profiling Float Array

T. M. Shaun Johnston[1], Daniel L. Rudnick[1], Noel Brizuela[1], and James N. Moum[2]

[1]Scripps Institution of Oceanography, University of California, San Diego, La Jolla, CA, USA, [2]College of Earth, Ocean, and Atmospheric Sciences, Oregon State University, Corvallis, OR, USA

Key Points:
- Over 20,000 subsurface temperature profiles were obtained before, during, and after a sequence of typhoons from an array of up to eight floats
- Two floats tracked the weakly stratified cold wake over 1,000 km westward in the North Equatorial Current
- Super Typhoon Yutu weakened into a typhoon before landfall, following its encounter with the previous typhoons' cold wake

Correspondence to:
T. M. S. Johnston,
shaunj@ucsd.edu

Citation:
Johnston, S., Rudnick, D. L., Brizuela, N., & Moum, J. N. (2020). Advection by the North Equatorial Current of a cold wake due to multiple typhoons in the western Pacific: Measurements from a profiling float array. *Journal of Geophysical Research: Oceans*, *125*, e2019JC015534. https://doi.org/10.1029/2019JC015534

Received 28 JUL 2019
Accepted 13 MAR 2020
Accepted article online 17 MAR 2020

Abstract Cold wakes of previous tropical cyclones (TCs) affect the development of subsequent TCs, but few subsurface data sets have sufficient persistence and spatial coverage to follow a cold wake as it is advected by currents. For >2 months in 2018, an array of eight floats obtained >20,000 temperature profiles from the surface to <200 m every <40 min before, during, and after Super Typhoons Mangkhut, Trami, Kong-Rey, and Yutu. Two floats were in/near Mangkhut's eye, experienced gale force winds during Trami and Kong-Rey, drifted over 1,000 km westward with the North Equatorial Current, and tracked the advection of the weakly stratified, cold wake produced by the sequence of TCs. Sea surface temperature shows the westward advection of the cumulative cold wake. While causation cannot be established, since atmospheric measurements were not made, Yutu weakened as it passed over the cold wake. The stratification and the energy needed to mix the water column in the cold wake decreased with each TC. One float directly in the path of Yutu showed that mixing to 125–150 m was likely, corresponding to a cooling of 0.5–1°C under the eye. Sea surface temperature in the cold wake cooled by 1°C within a 150 km radius of Yutu's eye, where the effect on air-sea heat fluxes is maximal. A cold wake can remain weakly stratified for many weeks during a sequence of TCs. These results also suggest that an advected cold wake from previous TCs may contribute many weeks later to the arrested development of a subsequent TC at a distant location.

Plain Language Summary Cold wakes from previous tropical cyclones (TCs) are known to affect the development of subsequent TCs, but few subsurface data sets have sufficient persistence and spatial coverage to follow a cold wake as it is transported by currents. For >2 months in 2018, an array of eight profiling floats drifted >1,000 km westward and tracked the weakly stratified, cold wake produced by a sequence of three TCs. The subsequent Super Typhoon Yutu weakened into a typhoon, as it passed over the cold wake prior to landfall. Coincidence occurred, but causation cannot be established, since detailed atmospheric measurements were not made. The stratification and thus the energy needed to mix the water column in the cold wake decreased with each TC. One float directly in the path of Yutu showed that mixing to 125–150 m was likely, corresponding to a cooling of 0.5–1°C under the eye, where the effect on air-sea heat fluxes that power TCs is maximal. These results show that a cold wake from previous TCs is transported by ocean currents to a distant location. The cold wake may possibly contribute many weeks later to the arrested development of a subsequent TC at a distant location.

1. Introduction

Tropical cyclone (TC) development depends on large-scale atmospheric conditions, internal TC dynamics, and air-sea heat exchange (Emanuel, 2003; Wang & Wu, 2004). Surface winds and air-sea temperature (T) differences drive these heat fluxes. The subsurface T structure indirectly contributes to TC intensification by its effects on sea surface temperature (SST). Warm mixed layers, deep thermoclines, and strong stratification limit vertical mixing of cool water, SST cooling, and downward air-sea fluxes (Balaguru et al., 2015; Lin et al., 2005, 2008; Mei et al., 2015; Wu et al., 2007). TC winds produce a cold wake of reduced SST via air-sea fluxes and upwelling, but more so by mechanical mixing of cooler water upward, arising from near-inertial current shear at the mixed layer base (Emanuel, 2003; Price, 1981, 2009; Wu et al., 2016).

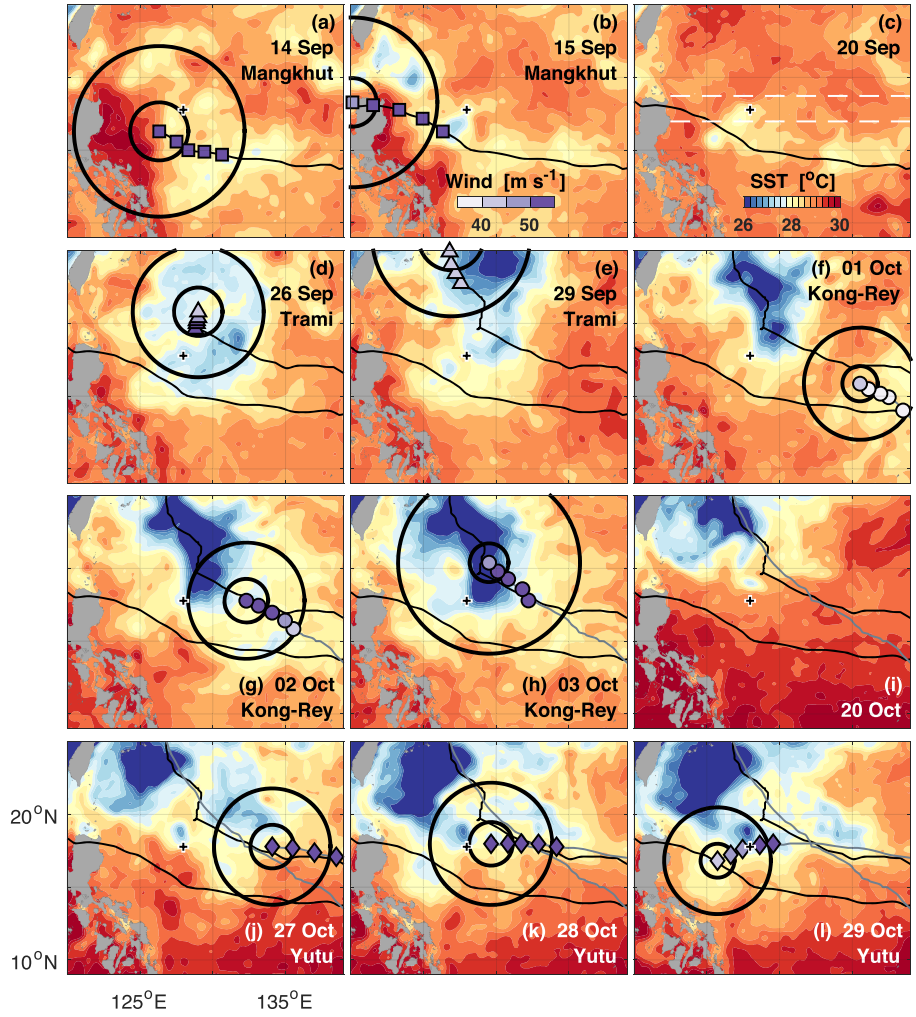

Figure 1. (a–h) SST shows cooling from the sequence of three TCs from 14 September to 3 October. (i) Warming occurred over the next 3 weeks as exemplified by SST on 20 October. (j–l) STY Yutu cooled SST from 27–29 October. Black and white cross denotes location where STY Yutu weakened into a typhoon. The time series at this location is in Figure 3g. TC names are noted, when their track (black and gray lines) cross the area. Inner/outer circles denote radii of storm/gale winds. Purple shading denotes maximum wind speeds from 0000 UTC at 6 hr intervals to the previous day at 0000 UTC, while the shape represents each TC (squares for Mangkhut, triangles for Trami, circles of Kong-Rey, and diamonds for Yutu; also in subsequent figures). Dashed white lines in Figure 1c along 16.975° and 18.725°N show location of Hovmöller plots in Figure 7.

After a TC passes by a given location in about 1–2 days, a cold wake's SST typically recovers in a few days. However, subsurface T can remain cool for weeks, be mixed upward during subsequent TCs, and again decrease SST (Baranowski et al., 2014; Balaguru et al., 2014; Brand, 1971; D'Asaro et al., 2014; Hart et al., 2007; Mrvaljevic et al., 2013; Wada et al., 2014). This TC-TC interaction via the ocean can act to decrease the intensity of subsequent cyclones, which encounter cold wakes (Balaguru et al., 2014). In a global simulation, incorporating a measure of the subsurface stratification along with a measure of wind power input to the ocean, improves statistical hindcasts of cold wake SST by 40% compared to wind power alone (Vincent et al., 2012). In comparison, metrics based on fixed thresholds or temperatures, such as heat content above the 26°C isotherm or the depth-mean T, only provide a 5% improvement. Changes in the subsurface ocean beneath a TC explain 32% of the variance in TC intensification rate at 3-day lead times in a model (Balaguru et al., 2015). The location of an existing wake directly under a subsequent TC's inner core exerts considerable influence- a 1°C change can decrease heat fluxes by 40% (Cione & Uhlhorn, 2003; D'Asaro et al., 2007). Furthermore, mesoscale eddies can advect cold wakes by hundreds of kilometers (Mrvaljevic et al., 2013). Persistent, subsurface observations (T, stratification, and mixed layer depth) tracking a cold wake are rare

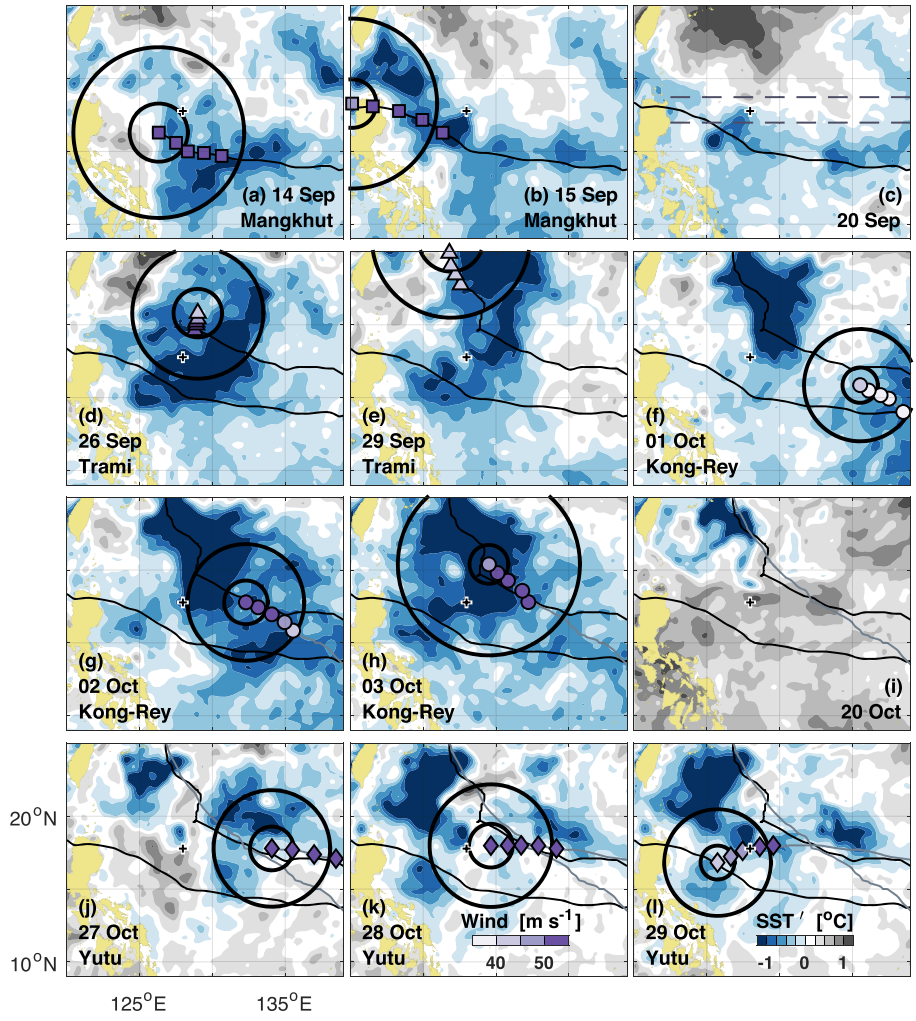

Figure 2. As in Figure 1 but for SST′.

to the best of our knowledge (Balaguru et al., 2014; Baranowski et al., 2014; D'Asaro et al., 2014; Mrvaljevic et al., 2013), but these data are critical for improved prediction.

In this paper, a sequence of four TCs cooled a wide area of the western North Pacific from 23 August to 9 November 2018 (Figures 1 and 2). An array of eight floats profiled every <40 min to <200 m and obtained >20,000 profiles at varying distances and under different wind conditions, which is rarely done (Black et al., 2007; D'Asaro et al., 2014). Super Typhoon (STY) Mangkhut was sampled best (Figure 3a), while other TCs were observed with fewer and more distant floats (Figures 3b–3d). These real-time, subsurface profiles were combined with real-time TC best track and wind data from the Regional Specialized Meteorological Center (RSMC), Tokyo (section 2) to understand the magnitude, extent, and duration of changes in the subsurface ocean (sections 3 and 4). Our main point is as follows: The subsurface ocean structure of a cold wake from previous TCs remained weakly stratified for weeks and was advected >1,000 km westward by the North Equatorial Current (NEC) to the point where STY Yutu weakened into a typhoon (section 5). We establish the coincidence of weakening over the cold wake but are cautious about ascribing causation because atmospheric measurements were not made. A summary follows (section 6).

In addition to our scientific point about the advection of the weakly stratified cold wake, our technical achievement is also noteworthy, as are the future implications. Our float array measured considerable and persistent changes in SST, subsurface T, mixed layer depth, and stratification underneath TCs at high vertical (one data point every ~0.1 m) and temporal (one profile every ~40 min) resolution over a wide area. While our extensive subsurface T measurements are comparable in density to previous work under

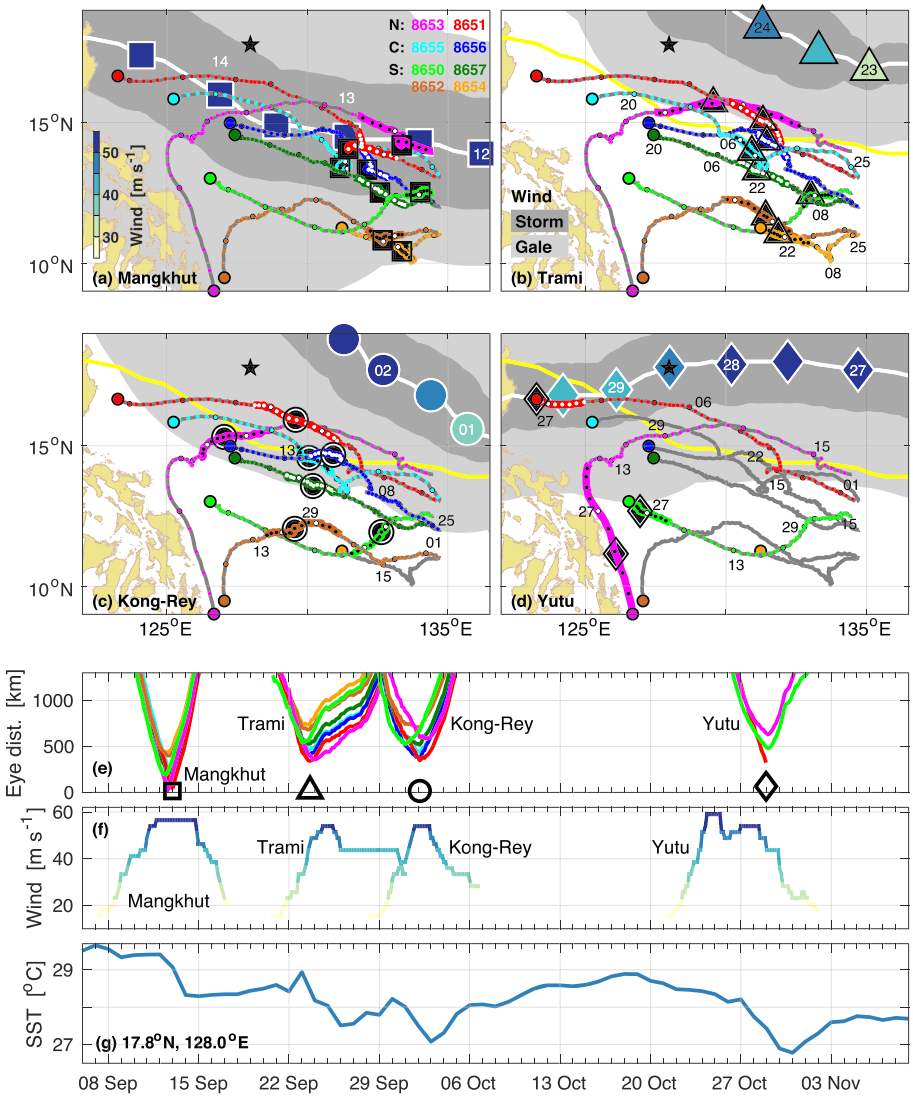

Figure 3. (a) STY Mangkhut's track (white line, yellow in other panels), radius of storm/gale force winds (dark/light gray), and maximum sustained wind speed (12-hourly colored squares with dates for 12–14 September) are shown over <3 days. On each float's trajectory (colored lines 7 days before/after each TC, gray lines otherwise) over >2 months, the daily positions at 0000 UTC are indicated by small colored dots and black circles correspond to weekly date labels (Figures 3e and 3f, and 4–6). Each float's closest position to the TC center (black square) and ending float positions are shown (large colored dots). (b–d) As in Figure 3a, but for Trami, Kong-Rey, and Yutu (triangle, circle, and diamond symbols). Some dates at some weekly float positions are shown on the maps in black. Float tracks are shown in gray if it is not operating during a TC. (e) The distance to the center of the TC is shown (colored lines for each float). The open symbols identify the time of closest approach for Float 8651 and are repeated in other figures for each float. (f) The maximum sustained wind speeds for each TC are shown as a function of time. Colors correspond to Figures 3a–3d. (g) SST time series at the point where STY Yutu weakened into a TY (black star, Figures 3a–3d).

Hurricane Frances (multiple profiling floats and surface drifters over several days Black et al., 2007; D'Asaro et al., 2007; Sanford et al., 2011), the combination of spatial extent, duration, and fine vertical and temporal resolution under or near a sequence of TCs is rare (D'Asaro et al., 2014; Mrvaljevic et al., 2013). Obtaining $\mathcal{O}$(10,000) profiles with such temporal resolution is possible via large multiplatform efforts (Black et al., 2007; D'Asaro et al., 2014) or arrays of multiple floats, which are air launched (Jayne & Bogue, 2017) or deployed by ship, as we did. Many other oceanic measurements represent only chance encounters of a few days or statistical analyses of global data sets. Such data will become more common with intentional and fortuitous placement of moorings, air-launched probes, surface drifters, gliders, and profiling floats (e.g., Baranowski et al., 2014; Black et al., 2007; Chang et al., 2016; Domingues et al., 2019; Jayne & Bogue, 2017; Lin et al., 2017;

Mitarai & McWilliams, 2016; Mitchell et al., 2005; Mrvaljevic et al., 2013; Pallàs-Sanz et al., 2016; Park et al., 2011; Price, 1981; Todd et al., 2018). Such data communicated in real time will increasingly contribute to forecasts (Chen, Cummings, et al., 2017; Domingues et al., 2019; Goni et al., 2017; Zhang & Emanuel, 2018).

2. Data

From 1959–2017, the mean annual number of typhoons (TY) in the western North Pacific was 17.2, including 4.3 STY (Bushnell & Falvey, 2017). From 9–26 TY have been noted in one calendar year, including 0–11 STY. In 2018, Joint Typhoon Warning Center (JTWC) reported 17 TYs in the western North Pacific, including seven STY and one TC that developed initially in the eastern Pacific. The effects of STY Mangkhut, Trami, Kong-Rey, and Yutu on the ocean are addressed here. STY and TY classifications are based on 1 min winds from the JTWC with TY wind speeds of 33–66 m s^{-1}, and STY winds >66 m s^{-1}.

Real-time data on each TC's track, sustained wind speeds, and the radii of gale and storm force winds are produced at 3-hourly intervals by the RSMC (Figure 3). Data were obtained via the Digital Typhoon website (Kitamoto, 2017). Substantial differences in wind speed (even after accounting for averaging time) and structure are noted for an individual TC between JTWC and RSMC (Knapp & Kruk, 2010; Song & Klotzbach, 2016). Since JTWC data were not immediately available, we used the RSMC data to provide timely locations of the TCs, extent of the winds, and wind speed. The best track data provide the center positions of the TCs. The sustained maximum wind speed at 10 m is a mean over 10 min (Figure 3f), while gale/storm force wind speeds are >15/26 m s^{-1} or 30/50 knots (from RSMC, which has different definitions than JTWC and the Beaufort scale). The radii are obtained by averaging the semimajor and semiminor axes (light/dark gray for gale/storm force winds, Figures 3a–3d). STY Mangkhut, Trami, and Kong-Rey all exhibited maximum sustained winds of 54–59 m s^{-1}. As STY Yutu crossed 130°E, it weakened into a TY with 44 m s^{-1} maximum sustained winds about 1 day before reaching a float directly in its path (Figures 3d–3f).

Our array of eight SOLO-II floats obtained T and salinity (S) profiles before, during, and after Mangkhut, Trami, Kong-Rey, and Yutu (Figure 3). To aid our discussion below, we identify northern, central, and southern groups of floats. The two northern floats experienced the greatest cooling from STY Mangkhut and Trami (8653 and 8651—pink and red lines denote these floats in all figures). The two central floats measured the most cooling during STY Kong-Rey (8656 and 8655—dark and light blue lines in all figures). The four southern floats were least affected by the TCs (8657, 8650, 8652, and 8654—dark green, light green, brown, and orange lines).

Our focus here is the upper ocean, and we programmed the floats to profile rapidly and continuously. SOLO-II floats are reliable, autonomous, Lagrangian platforms designed and built by the Instrument Development Group at Scripps and are extensively used in the Argo program (Davis et al., 2001). On each dive cycle, a float obtains a starting position from the Global Positioning System at the surface, descends to a target depth, then ascends taking measurements at 1 Hz on the upward profile, obtains an ending position, transmits data via Iridium satellite, and then begins another cycle. Since a float moves with the depth-mean current over its profiling range, it is neither Eulerian nor Lagrangian with respect to the surface layer (defined in the following paragraph). Given that velocity generally decreases with depth, we expect that the floats moved more slowly and in a different direction than the surface layer. The maximum profiling depth for the floats ranged from 80–200 m, with a full cycle taking 22–40 min at vertical profiling speeds of 0.12 m s^{-1}. After two groups of three floats had already been deployed from R/V *Thomas Thompson* at 11°N, 12°N, and 13°N along 134.75°E, STY Mangkhut was forecast to pass to the north of the array. To sample within the approaching TC, Float 8653 was placed along the predicted path at 14°N, 134.5°E and Float 8650 was placed closer to the rest of the array at 12.5°N, 134.5°E (Figure 3a).

For each profile, the isothermal layer depth (ITLD) is defined as the depth where T decreases by 0.5°C from its value at 10 m (similar to Sprintall & Tomczak, 1992). By avoiding the upper 10 m, we limit the influence of prominent diurnal heating near the surface (Figure 4). The exact details of the ITLD definition minimally change our results because the mixed layer base has a vertical extent with large gradients (e.g., Johnston & Rudnick, 2009). The mean ITLD for the eight floats ranges from 48–68 m.

While atmospheric conditions account for much of TC intensity changes, the subsurface structure can contribute indirectly to the SST under the TC's eye. We consider two measures of subsurface T and stratification: the heat content anomaly (H) and available potential energy (APE). H reflects the changes over time in the

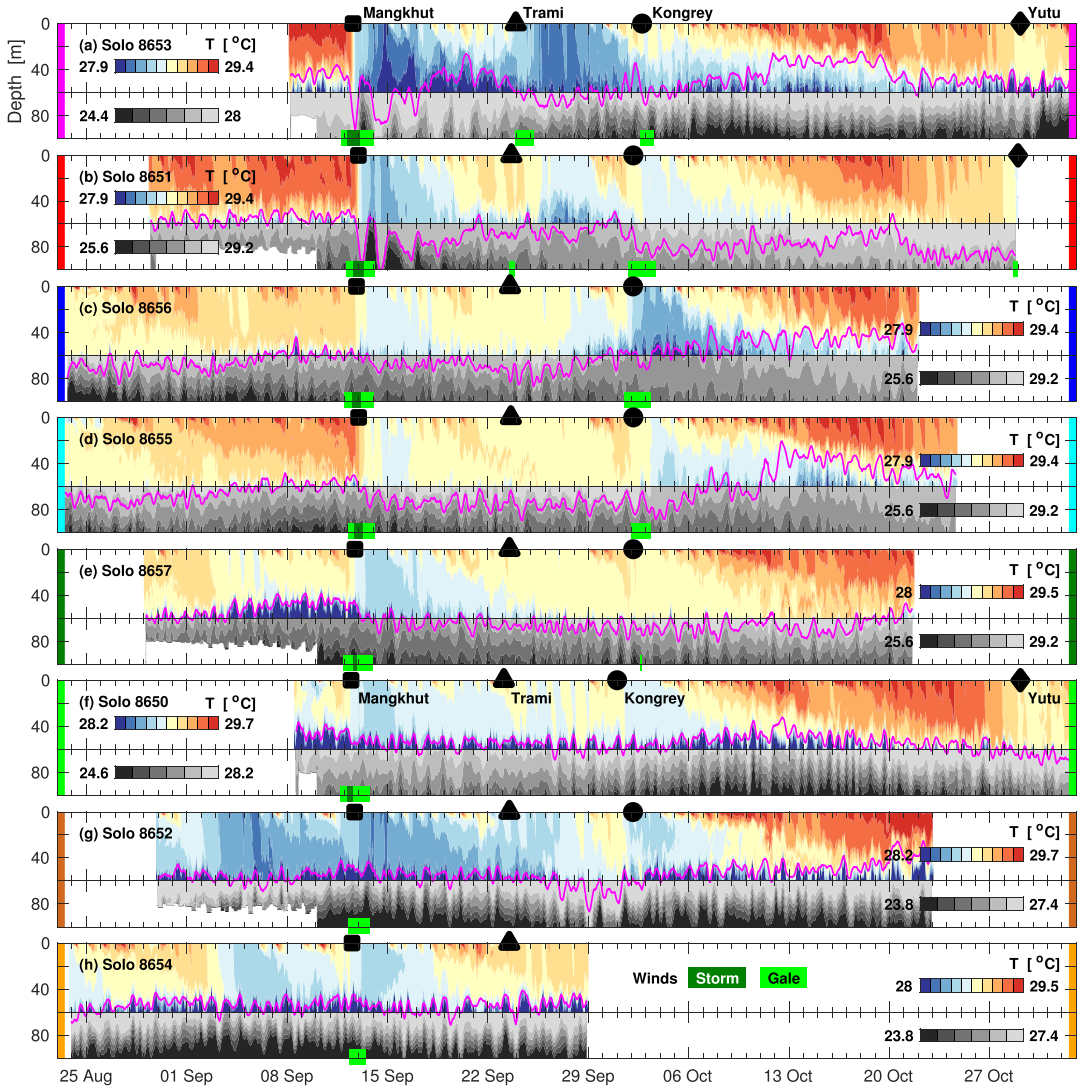

Figure 4. Temperature measured by the eight floats—(a) 8653, (b) 8651, (c) 8656, (d) 8655, (e) 8657, (f) 8650, (g) 8652, and (h) 8654. To emphasize and compare changes in the upper ocean, the T range is a constant 1.5/3.6°C in the colored/gray shading from 0–60/60–100 m. The deeper T data and ITLD (pink line) are smoothed over 0.75 days. The times of closest approach for STY Mangkhut, Trami, Kong-Rey, and Yutu to each float are denoted by symbols (square, triangle, circle, and diamond). Dark/light green shading highlight the duration of storm/gale force winds at each float for each TC. Vertical bars at the ends of each panel reference each float's color in all figures.

integrated T of the upper ocean (but not its stratification) and is obtained from the temperature anomaly (T') as $H_h(t) = \langle\rho\rangle C_p \int_{-h}^{0} T'(z,t)\, dz$, where z is the vertical coordinate, $\langle\rho\rangle$ is the mean in situ density over the depth (h = 50 and 75 m, similar to the range of mean ITLD) and time (t) of the observations, and C_p is the specific heat capacity. The temperature anomaly is calculated with respect to the mean profile: $T'(z,t) = T(z,t) - \bar{T}(z)$. Mean values are evaluated before the arrival of STY Mangkhut using data from 0400 UTC on 10 September to 0000 UTC on 12 September 2018, which is almost an inertial period—49 hr at 14°N. By examining depth-time sections of T', we note cooling in the upper ocean during and after the TCs (Figure 5). T' usually shows negative values above 60 m for the four northern and central floats. Since the mean ITLD for the eight floats varies from 48–68 m, we use 50 and 75 m as integration limits for calculating H (Figure 6). Internal wave activity is higher in the thermocline—that is, below the ITLD. The qualitative differences between H_{50} and H_{75} are minor. H is often calculated to the depth of the 26°C, but TC intensity change in the deep ocean is better correlated with metrics including either a depth-mean T, an integration of T over a fixed depth, or stratification (Lee et al., 2019; Price, 2009; Vincent et al., 2012).

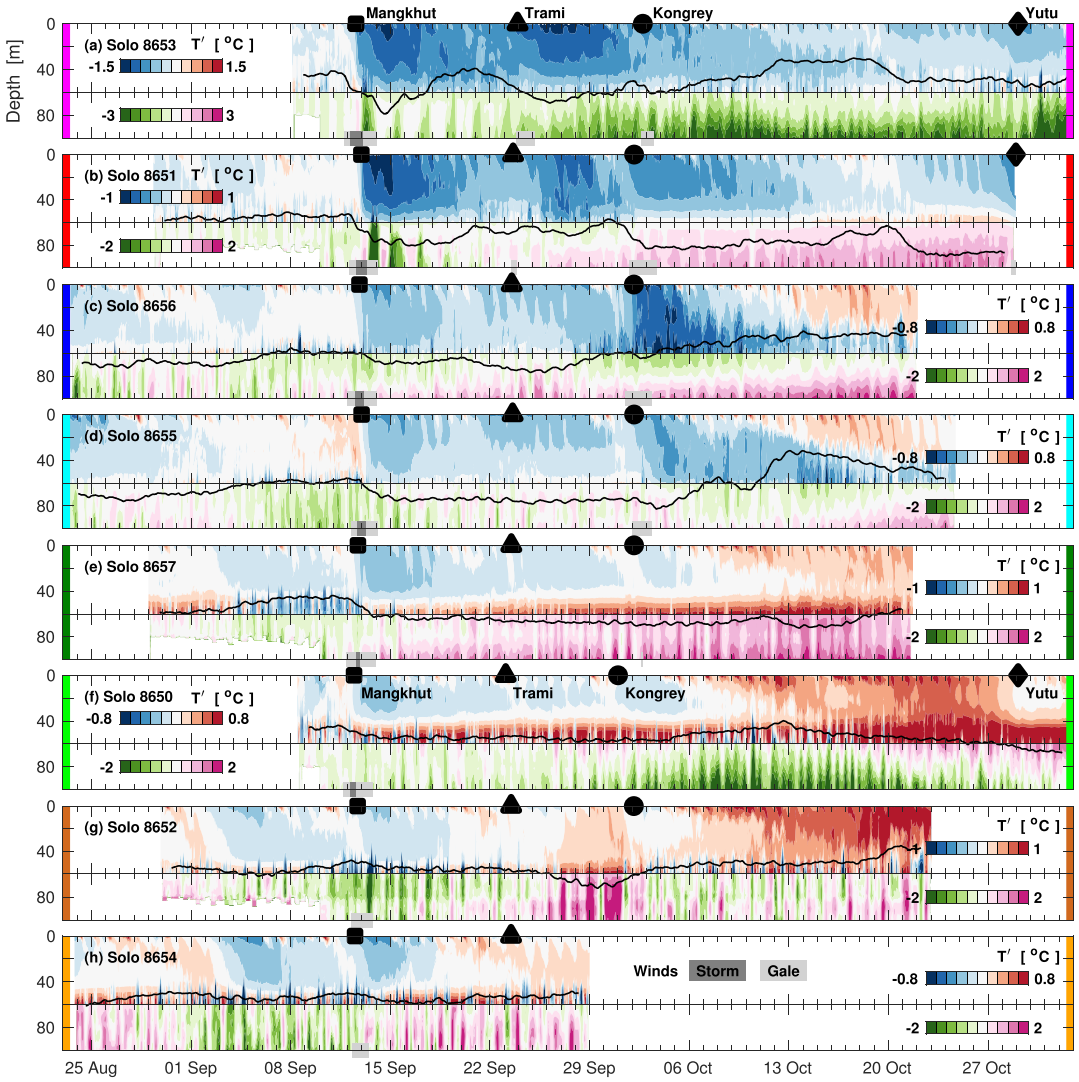

Figure 5. As in Figure 4, but for T'. ITLD is smoothed over 1.5 days (black line). Note the variable ranges for T'.

Available potential energy (APE) is the energy required to mix the water column and accounts for stratification. It is the difference between the initial and mixed (or final) potential energies: $APE_h(t) = \int_{-h}^{0} [\langle \sigma_\theta \rangle - \sigma_\theta(z,t)]\, g\, z\, dz$, where $\sigma_\theta(z)$ is the observed potential density profile prior to mixing, $\langle \sigma_\theta \rangle$ is the depth-mean or final potential density calculated from the mean or mixed values of T and S over depths h = 75–150 m, and g is the gravitational acceleration (Vincent et al., 2012). Our observations demonstrate the utility of APE in understanding the cooling from three previous TCs in 2018 underneath STY Yutu prior to landfall, which coincided with its weakening into a typhoon. These cool, deep, and weakly stratified wakes were advected about 1,000 km westward by the NEC over 6 weeks and APE decreased with each TC.

We use two heat flux products and an SST product. The mean net heat fluxes from the ERA-Interim global atmospheric reanalysis from the European Centre for Medium-Range Weather Forecasts help evaluate how long the ocean takes to recover from the heat loss due to a TC (Dee et al., 2011). These results are linearly interpolated in space and time onto the trajectory of float 8653. The OAFlux product provides very similar results in the mean as expected for large-scale warming (Yu & Weller, 2007).

The Group for High-Resolution SST produces an optimally interpolated SST from multiple satellite and in situ measurements (Donlon et al., 2007), which we use to evaluate cooling over a wider area than measured by the floats during the first three TCs and during the weakening of STY Yutu into a TY. These data are on a grid, which is 0.05° in space and daily in time. To account for a seasonal signal at each spatial location (which

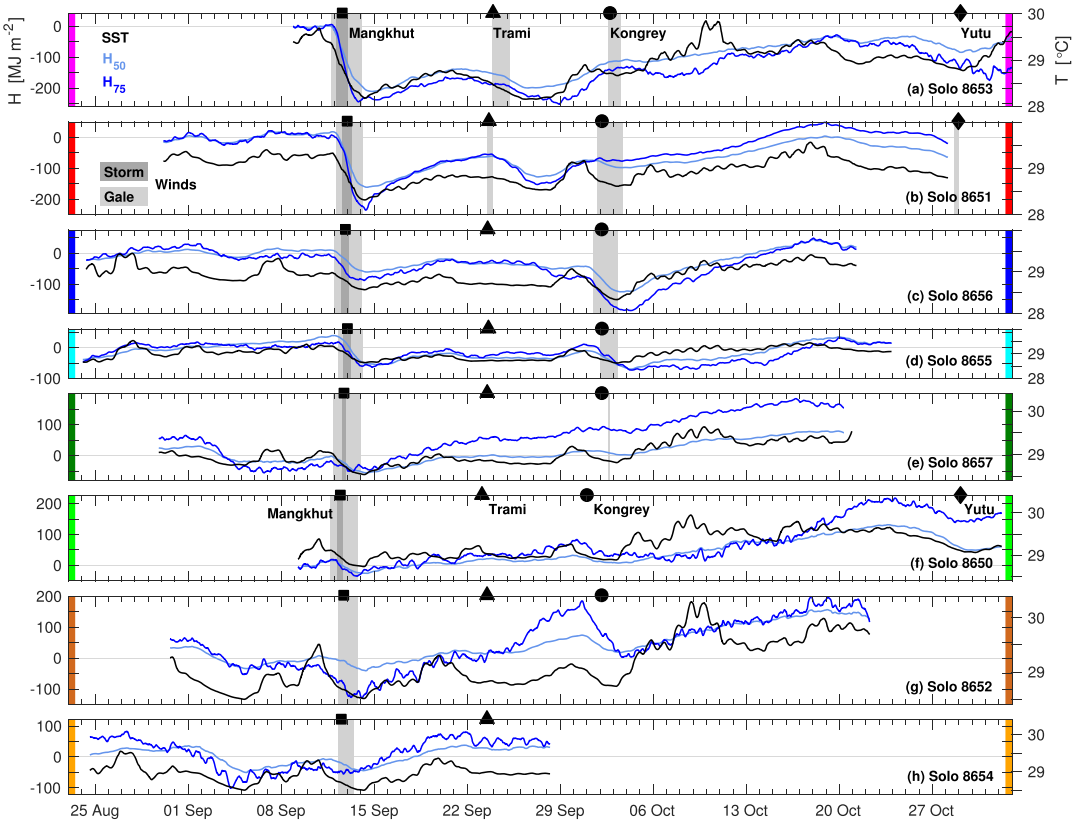

Figure 6. SST (black), H_{50} (light blue), and H_{75} (dark blue) are smoothed over 1.5 days to minimize internal wave effects for the eight floats in order from north to south during the passage of STY Mangkhut—(a) 8653, (b) 8651, (c) 8656, (d) 8655, (e) 8657, (f) 8650, (g) 8652, and (h) 8654. The vertical scale is constant for H, but the T scale covers a constant range from 28–29.9°C. The times of closest approach for STY Mangkhut, Trami, Kong-Rey, and Yutu to each float are denoted by symbols (square, triangle, circle, and diamond). Dark/light gray shading highlight the duration of storm/gale force winds at each float. Vertical bars at the ends of each panel reference each float's colors in all figures.

is small compared to SST variability from the TCs), we remove a trend from 1 August to 30 November 2018 and compute the anomaly, SST′, which is useful in some of the figures to follow. Since SST measurements are obscured by rain in the inner core (Wentz et al., 2000), we average time series data under TCs over a radius >150 km. Maps are shown without any averaging, since we are interested in broad spatial patterns.

3. Ocean Cooling by a Sequence of TCs

SST cooled over a wide area during the four TCs. SST was >29°C prior to Mangkhut (Figure 1a), which lowered SST by >1°C for more than 1 week (Figures 1a–1c and 2a–2c). STY Trami and Kong-Rey followed similar tracks from 26 September to 3 October through our study area and again caused >1°C cooling across the whole area (Figures 1d–1h and 2d–2h). Kong-Rey intensified the cooling over a wider area. SST warmed for the next 3 weeks except for a patch in the northwest corner of the area that remained cool (Figures 1i and 2i). As STY Yutu arrived on 27 October, cooling occurs over a wide area again, the patch in the northwest corner cools further, and cooling is noted to the right of the TC track (Figures 1j–1l and 2j–2l). On 28–29 October, Yutu weakened into a typhoon near 17.8°N, 128°E (black and white cross in Figures 1 and 2 and with purple symbols indicating wind speed).

The TCs moved westward rapidly at >5 m s^{-1} or >400 km day^{-1} (Figures 3a–3d), while the float array drifted westward with the NEC at a mean speed of 0.18 m s^{-1} or 16 km day^{-1}. Thus, individual floats experienced the strongest winds for only 1–2 days (Figures 3e and 3f). Despite the rapid passage of the TCs, they produced lasting effects on the ocean. SST decreased by about 1°C after each TC at a representative site (Figure 3g). Persistent cooling from each TC (~1 week) and the sequence of TCs (>1 month) is notable as the northern

and central floats drifted with the cold wake in the NEC. The four southern floats measured some cooling during Mangkhut and warming thereafter. Next, we consider the effects of each TC in detail.

STY Mangkhut was best sampled by the array, which was mostly to the left of the TC (Figure 3a). The two northern floats (pink and red lines, Figure 3a), were within 21 and 46 km of the TC's center position, with one likely within the eye, which at this point had a radius of 25 km (Joint Typhoon Warning Center, 2018). These floats slowed or reversed direction during STY Mangkhut, which indicates that the depth-mean current became eastward under eastward winds to the left of the eye (Figure 3a). Two central (dark and light blue) and two southern (dark and light green) floats were within the radius of storm force winds, while the two southernmost (orange and brown) floats experienced gale force winds. The isothermal layer cooled by up to 1.2°C at the northern floats between 12 and 15 September (squares, Figures 4a and 4b, and 5a and 5b). The corresponding change in heat content from 1 day before to 1–2 days after the closest approach of Mangkhut was largest at the northern and central floats with $\Delta H_{50} \approx -200$, -175, -75, and -100 MJ m^{-2} (Figures 6a–6d). The greatest heat losses were observed at the two northern floats, which were near or within the eye. The southern floats were farther left of the TC track and showed smaller changes: $\Delta H_{50} \approx -50$ MJ m^{-2} (Figures 6e–6h). H is smoothed over 1.5 days to reduce the effects of internal waves (Figure 6), but neither T nor T' above 60 m in the time-depth sections are smoothed (Figures 4 and 5).

Next, we compare our measurements to previous estimates of heat loss under TCs and turbulent heat flux across the mixed layer base. The float array was mostly on STY Mangkhut's left side and measured an SST drop of 1–1.2 °C, likely less than the maximum cooling on the right side of this fast moving TC (Price, 1981). The heat flux was about 3.5 kW m^{-2} (150 MJ m^{-2} of cooling occurred over 12 hr in the unsmoothed data in the upper 50 m at the northern Float 8653 during STY Mangkhut; 1.5 day running means are in Figure 6). For comparison, during Hurricane Frances, float and drifter measurements showed SST cooled by up to 2.2°C (1°C) to the right (left) of the track, which corresponds to a heat loss of 600 (200) MJ m^{-2} over about 6 hr or a flux across the mixed layer base of 25 (8) kW m^{-2} (D'Asaro et al., 2007). For floats in the Argo array within the radius of gale force winds of category 4–5 TCs, a statistical analysis found a mean mixed layer loss of 160 MJ m^{-2}, a recovery time of more than 30 days, and a SST recovery time of about 1 week (Park et al., 2011). In our observations, even though H_{50} recovered more quickly, the sequence of TCs left a weakly stratified wake, which is addressed in the next section.

When STY Trami arrived 11 days later on 23 September, neither T nor H had recovered to pre-Mangkhut values at the northern and central floats (Figures 4a–4d, 5a–5d, and 6a–6d). STY Trami's propagation slowed considerably for the next 4 days (Figures 3e). At closest approach, Trami was about 400 km distant from the two northern floats, which experienced gale force winds (light gray shading, Figure 3b) causing further heat loss of about 50 MJ m^{-2} (Figures 6a and 6b). The two central floats showed little change in T and H during Trami (Figures 4c and 4d, and 6c and 6d).

STY Kong-Rey intensified and expanded its radius of gale force winds just as it passed over the two northern and two central floats on 2 October (Figure 3c). The radius of gale force winds was 445 km and then grew over the next 18 hr to 740 km as the maximum winds increased from 39 to >55 m s^{-1} (Figures 3c, 3e, and 3f). At the two central floats, which were closest to Kong-Rey, T decreased >0.5°C (Figures 4c and 4d, and 5c and 5d) and ΔH_{50} was -100 and -50 MJ m^{-2} (Figures 6c and 6d). No appreciable cooling was noted at the northern and southern floats in H_{50}, but warming trends were reduced substantially (Figures 6a and 6b, and 6e and 6f). Kong-Rey weakened on 3 October, as it encountered the cold wake from Trami (Figures 1h and 3; section 5).

STY Yutu had weakened to TY status before reaching the floats and its effects were measured at one float inside the gale radius and two floats outside it (Figure 3d). On 28 October, T decreased by 0.5°C during TY Yutu at the last active floats (8653, 8651, and 8650; Figures 4a, 4b, and 4f) with ΔH_{50} of -100 to -50 MJ m^{-2} over a few days (Figures 6a, 6b, and 6f). Averaged over a 150 km radius around the point where Yutu became a typhoon, a decrease of 1°C in satellite SST to 27°C was noted after TC passage (Figure 3g). Further weakening of Yutu occurred on 29 October over a region with a deeper ITLD (80 m, the deepest in our measurements; Figure 4b) and cooler T. This float coincidentally ran out of battery power 1 day before Yutu arrived and so the full ocean response under the eye was not measured, but decreasing T and H are noted. The weak stratification is consistent with mixing and the T decrease (section 5).

In summary, a sequence of three TCs over 3 weeks cooled the ocean at the northern and central floats by 0.5–1.2°C with corresponding ΔH_{50} of −200 to −50 MJ m^{-2} (Figures 4a–4d and 6a–6d). This cooling persisted for >1 month and covered a wide area, which, based on our observations, was likely all of the area under strong winds (gray shaded area, Figure 3). The SST over this area and H_{50} at the some northern and central floats recovered in mid-October (Figures 2 and 6b–6d; section 4). However, H_{50} at one of the northern floats (8653), which passed under Mangkhut's eye, never recovered to its pretyphoon level (Figure 6a). Almost 4 weeks after the passage of STY Mangkhut, Trami, and Kong-Rey, STY Yutu weakened into a typhoon as it passed over the wake from the sequence of TCs. Due to the position of the floats, our results are likely underestimating the contributions of STY Trami and Kong-Rey to the cold wake under Yutu's track. Further examination of the subsurface structure under Yutu follows in section 5 and focuses on the decreasing APE in the cold wake from each TC at one of the northern floats (8651), which was directly in the path of Yutu's eye.

4. Net Surface Heat Flux Into the Cold Wake

Cooling depends more on local, oceanic conditions and the location with respect to each TC. The turbulent subsurface heat flux across the mixed layer base was estimated in the previous section for STY Mangkhut. After the passage of Mangkhut, the net surface heat flux along the path of Float 8653 is evaluated with the ERA interim reanalysis product. We assume this warming is set by the large-scale conditions. We also neglect ongoing mixing across the mixed layer base and advective effects. From 15 September (H_{50} is minimum) to 20 October (H_{50} recovers almost to 0), the mean values of the latent heat flux, sensible heat flux, and net solar radiation from the reanalysis are −116, −7, and 220 W m^{-2} (positive values indicate ocean warming), which yields a mean total flux of 97 W m^{-2} with similar results from OAFlux. With reduced SST and thus increased air-sea T difference after each TC, these heat fluxes were likely higher in reality than in the reanalysis, which does not resolve the cold wake well. Larger values are noted for about 1 day after the TC in OAFlux, but with little effect on the mean over the 1 month warming. This heat flux is a small fraction of the flux during a TC. Thus, recovery of the oceanic T occurs over a period of days to weeks. As a rough indication, if this flux of 97 W m^{-2} were the sole source of warming, then the 200 MJ m^{-2} heat loss measured at Float 8653 would require 24 days for recovery (Figure 6a).

A linear recovery time of 1–3 weeks for a single TC comes from a linear extrapolation of warming trends seen after each TC at the two closest floats to STY Mangkhut (Figures 6a and 6b). For Float 8653/8651, the e-folding scale for H_{50} is 14/8 days, while the SST anomaly has decay scales of 11/8 days, all of which have standard errors of <0.5 day. The differences between a linear and exponential fit are negligible over our short observational interval between STY Mangkhut and Trami (15–21 September). Previously, the e-folding recovery time of the SST anomaly in cold wakes was calculated from a one-dimensional heat budget to be 5–20 days under different atmospheric conditions and comparable to observations (Price et al., 2008). This recovery depends on the air-sea heat flux anomaly over the cold wake, which depends on atmospheric parameters (e.g., winds, air temperature, humidity, and incident solar radiation) and oceanic parameters (e.g., SST, diurnal warming amplitude, and stratification). With a cold wake anomaly of 2 °C under weak post-TC winds of 5–7 m s^{-1}, their formulation of the decay scale yields 8–16 days, which suggests air-sea fluxes are primarily responsible for our observed increase of H_{50} with a decay scale of 8–14 days. However, since there were three TCs over 3 weeks, a full recovery was not observed (a similar situation to Price et al., 2008).

5. Weakening of STY Yutu Over the Cold Wake of Prior Typhoons

STY Yutu weakened suddenly to typhoon status on 28–29 October, as it moved westward past 130°E and over cooler water (Figures 1i, 3d, and 3f). This section examines SST and subsurface structure to show (a) the cumulative cold wake from previous TCs was advected westward in the NEC (D'Asaro et al., 2014; Mrvaljevic et al., 2013) and (b) APE decreased with each TC, rendering the water column susceptible to further mixing and cooling under Yutu. As noted in the introduction, both the atmosphere and ocean contribute to TC development, but we cannot determine the causes for Yutu's weakening due to the lack of atmospheric data.

The northern (8651 and 8653) and central floats (8655 and 8656) tracked the cold wakes from STY Mangkhut, Trami, and Kong-Rey from 12 September until 20 October along their 2000 km and 1,200 km trajectories, as they drifted westward with the NEC and into the southward Mindanao Current (Figures 3 and 6). The mean

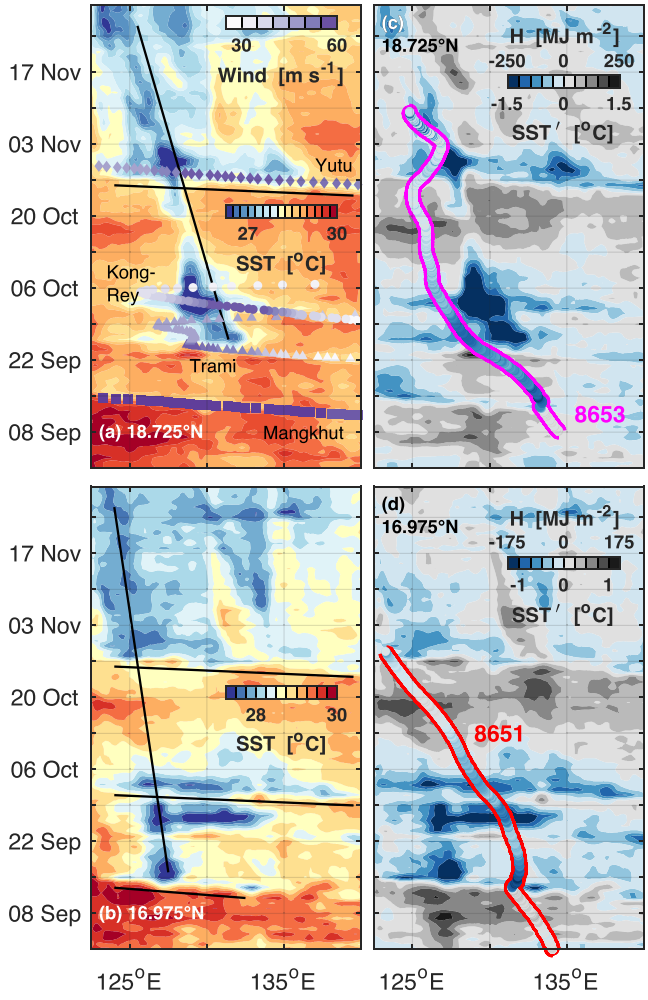

Figure 7. (a) Hovmöller plot of SST along 18.725°N shows cooling from four TCs. TCs propagate across the area in a few days (e.g., cooling due to STY Yutu's westward propagation is highlighted by the black line with a shallow slope), while ocean currents advect SST westward over many weeks (black line with steep slope shows SST advection by the NEC). TC wind speed is noted at the appropriate times and longitudes (purple squares, triangles, dots, and diamonds for STY Mangkhut, Trami, Kong-Rey, and Yutu), even though the latitude of the TC was different. STY Yutu weakened into a TY on 28–29 October over the cool water. (b) As in Figure 7a, but for SST along 16.975°N. Black lines with a shallow slope highlight STY Mangkhut, Kong-Rey, and Yutu. (c) As in Figure 7a, but for SST′ along 18.725°N. H_{50} from a northern float is plotted within the colored line at appropriate times and longitude, even though the float was at a different latitude. Note the float's propagation speed was often similar to the SST advection speed. (d) As in Figure 7b, but for SST′ along 16.975°N.

westward speed of the northern floats in the NEC was 0.25 m s^{-1}. We focus on the trajectory of one of the northern floats (8651) because it was directly in the path of TY Yutu prior to landfall (red, Figure 3d). The weak vertical T gradient seen by float 8651 (as noted by the deep ITLD) persisted for 1.5 months following STY Mangkhut (Figure 4b) across a distance of 1,200 km (Figure 3). A mismatch in oceanic and atmospheric scales is apparent in Figure 3 (daily positions are denoted with small dots along float trajectories and large symbols on TC tracks). Each TC passes through the domain in about 2 days and cools the ocean, while a float moves at most 100 km over this time and tracks water that remains cool for a week or more. The persistence of the oceanic heat loss is relevant to subsequent TCs.

Widespread cooling is apparent in SST (Figures 1 and 2), but it is difficult to see the westward propagation of the SST signal. In Figure 7, Hovmöller diagrams highlight this signal at two latitudes (18.725 and 16.975°N, dashed lines in Figures 1c and 2c), which are north and south of the point where Yutu weakened (black cross, Figures 1 and 2). Two distinct propagation speeds are noted: TCs crossed the area in about 3 days

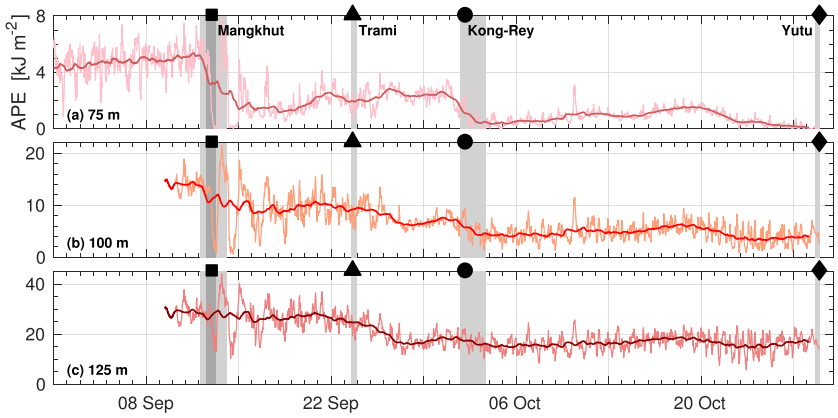

Figure 8. APE (thin lines) is integrated over (a) 75, (b) 100, and (c) 125 m for Float 8651, which was directly in the path of Yutu on 28–29 October when it weakened (red line, Figure 3d). APE averaged over 1.5 days (thick lines) decreases with TC passage prior to Yutu.

(black lines with shallow slopes in Figures 7a and 7b; purple symbols indicate wind speed for each TC), while ocean currents advected SST over many weeks (black lines with steep slopes in Figures 7a and 7b).

The passage of STY Trami and Kong-Rey cooled SST on the northern zonal line. On 3 October, Kong-Rey weakened over the cold wake of Trami (Figures 1h and 7a). The cold wake then moved steadily westward in the NEC throughout the record (steep black line, Figure 7a). The intersection of the two SST signals from the advected cold wake and the cooling from Yutu is the site of <1.5°C cooling on Yutu's track (intersection of the black lines in Figure 7a) on 29 October (Figures 1l and 2l). At this point, STY Yutu weakened into a typhoon (purple dots indicate wind speed in Figure 7a). The cold wake persisted for at least 10 weeks in the SST record, as it propagated farther west. On the southern zonal line, STY Mangkhut, Trami, and Kong-Rey produced cooling along the same characteristic (Figure 7b). Then SST warmed for 2 weeks before STY Yutu, during which maximum cooling was again along a characteristic linking the four TCs over 11 weeks. While the SST recovered over the 2 weeks prior to Yutu, pre-Mangkhut values of H_{50} were not reached at the northern floats (Figures 6a and 6b and 7c and 7d). Also, the large ITLD indicates stratification remained weak ahead of Yutu (Figure 4b). In summary, the sustained cooling from STY Mangkhut, Trami, and Kong-Rey propagated with the NEC. When STY Yutu passed over the advected cold wake, maximum cooling under Yutu's track is noted.

With each TC passage, APE measured the reduction of stratification and, thus, energy required to mix the upper ocean. Even though SST recovered over much of the study area before the passage of Yutu (Figure 1), the subsurface T gradient remained weak at the northern float (8651) directly in the path of Yutu (red; Figures 3d and 4b). STY Mangkhut, Trami, and Kong-Rey brought APE to 0 in the upper 75 m and close to 0 in the upper 100 m, indicating the water column was mixed to these depths (thick line, Figures 8a and 8b). The unsmoothed data show one TC passing directly over the floats was sufficient to accomplish this mixing (thin lines, Figures 8a and 8b). In the upper 125 m, Mangkhut reduced APE from its prestorm mean of 30 kJ m^{-2} (thick line, Figure 8c) by about 20 kJ m^{-2} in the unsmoothed data (thin line, Figure 8c). Trami reduced the mean APE to 20 kJ m^{-2}, which suggests that a direct encounter with Yutu may have been sufficient to mix the ocean to 125 m.

Since this float (8651) in the path of Yutu ran out of battery power just before the TC's passage, we estimate the potential cooling expected directly under Yutu by comparing to the previous cooling experienced directly under Mangkhut. Just prior to Yutu, mixing must reach 125, 150, and 175 m to cool the upper ocean by 0.5, 1, and 1.5°C (Figure 9). During Mangkhut, as the thermocline was heaved vertically, 1/1.5°C of cooling was obtained with mixing from 75–150/100–175 m (Figures 9b and 9c). With similar variability of the thermocline under Yutu, mixing to 150 m and cooling of 1°C could occur. These calculations of APE and mixing depth explain the 0.5–1°C cooling seen directly under Yutu in the SST product (Figures 1l, 2l, 3g, and 7). With each passing TC, APE decreased toward 0, suggesting that the stratification presented little barrier to mixing directly under Yutu near the site of its weakening.

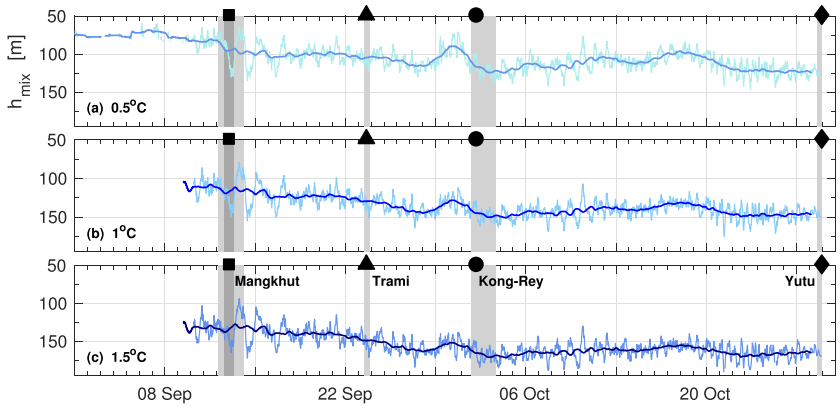

Figure 9. For upper ocean cooling of (a) 0.5, (b) 1, and (c) 1.5°C, the depth of mixing (thin lines) is calculated for Float 8651, which was directly in the path of Yutu on 28–29 October when it weakened (red line, Figure 3d). These depths are also averaged over 1.5 days (thick lines).

6. Summary

A sequence of three TCs produced a cold wake, which was advected >1,000 km by the NEC over 6 weeks in 2018 in the western Pacific into the path of a fourth TC, STY Yutu. An array of eight profiling floats obtained over 20,000 profiles to <200 m every <40 min under or near these TCs, which, to the best of our knowledge, is a rarely achieved coverage in time and space of an advected cold wake at high vertical and temporal resolution (D'Asaro et al., 2014; Mrvaljevic et al., 2013). Even though each of STY Mangkhut, Trami, and Kong-Rey passed over the sampled area in about 2 days, the ocean cooling persisted and had a linear recovery time of 1–3 weeks. Due to the more distant position of the floats during STY Trami and Kong-Rey, our results likely underestimate their effects on the cold wake under Yutu. After encountering this wake on 28–29 October, STY Yutu weakened into a typhoon prior to landfall. We have shown coincidence of cool SST and TC weakening but have neither addressed atmospheric contributions nor proven causation.

Cool SST directly beneath a TC's eye is more effective at reducing air-sea heat fluxes (Chen, Elsberry, et al., 2017; Cione & Uhlhorn, 2003; D'Asaro et al., 2007). STY Yutu's pressure decreased by about 40 hPa over 1 day when it weakened into a TY. Idealized coupled air-sea models of a TC encountering various cold wakes (changes of SST = 2°C, SST = 1°C, or mixed layer depth = 50 m, which are similar to our observations) produce changes of the TC's central pressure of 40, 15, and 20 hPa over 1, 2, and 2 days compared to control simulations (Chan et al., 2001; Chen, Elsberry, et al., 2017). Subsurface ocean conditions contribute considerably to the variance in predicted TC intensification rate (Balaguru et al., 2015). APE is a measure of energy required to mix the ocean to a certain depth, which incorporates the stratification. Each TC in our record reduced APE, which is a better predictor of SST cooling than heat content (Vincent et al., 2012). APE measured by one float ahead of Yutu suggests the stratification presented little impediment to mixing to a depth of 125 m or more, which could produce 0.5–1°C of cooling directly under the eye. Such cooling was noted in an SST product, but the float coincidentally ran out of power at this time and was unable to confirm the subsurface cooling. The cumulative effect from the sequence of four TCs produced a sustained cooling observed by the floats for 4–7 weeks and in the longer SST record over 10–11 weeks. Such an advected cold wake from previous typhoons may contribute to the SST cooling beneath subsequent typhoons and affect their development at distant locations and later times.

STY Mangkhut was particularly well sampled by the array. Two floats were within 21 and 46 km of the TC's center position. The closest float measured cooling in the upper 50 m of 3.5 kW m^{-2}. It was probably within the eye, which had a radius of 25 km on 13 September. Another four (two) floats were within the radius of storm (gale) force winds. This TC is examined in greater detail by Brizuela et al. (Three-dimensional diagnosis of turbulent mixing and internal wave generation under a tropical cyclone, personal communication, 14 Feb 2020). While TC intensity is sensitive to air-sea fluxes (Chen et al., 2018), often upper ocean conditions are not well initialized in operational, coupled TC models (Zhang & Emanuel, 2018). Thus, these high-resolution subsurface data from the profiling float array may prove useful in better understanding the air-sea heat exchange of a TC in coupled models or via data assimilation (Domingues et al., 2019; Chen, Cummings, et al., 2017; Chen, Elsberry, et al., 2017; Zhang & Emanuel, 2018) because the array measured

SST and subsurface T on time and space scales relevant to the TC. Supplementing the Argo float array with additional floats intended to observe TCs may be one way to achieve similar high-frequency profiles in the path of a TC far from land. The additional floats themselves may not encounter a TC but could be exchanged for existing floats along a predicted track. The selected floats could then profile rapidly in the upper ocean.

Acknowledgments
This work is supported by Grant NA17OAR4310259 from the Climate Variability and Predictability program at NOAA and N00014163085 from the Office of Naval Research's PISTON initiative, which are components of the international Years of the Maritime Continent program. We are grateful to the master, crew, and science party on R/V *Thomas Thompson* for their help in deploying the floats. The Instrument Development Group at the Scripps Institution of Oceanography designed, prepared, and monitored the SOLO-II floats. Typhoon data are produced by RMSC at the Japan Meteorological Agency and were downloaded from https://www.digital-typhoon.org/. GHRSST data were downloaded from the Asia-Pacific Data-Research Center (at https://apdrc.soest.hawaii.edu/). Float data are available at the PISTON data site (at https://www-air.larc.nasa.gov/cgi-bin/ArcView/camp2ex?TRAJECTORY=1#JOHNSTON.SHAUN/). Adam Sobel provided insightful comments on earlier versions of the manuscript. We thank three anonymous reviewers for their helpful comments.

References

Balaguru, K., Foltz, G. R., Leung, L. R., D'Asaro, E., Emanuel, K. A., Liu, H., & Zedler, S. E. (2015). Dynamic potential intensity: An improved representation of the ocean's impact on tropical cyclones. *Geophysical Research Letters*, *42*, 6739–6746. https://doi.org/10.1002/2015GL064822

Balaguru, K., Taraphdar, S., Leung, L. R., Foltz, G. R., & Knaff, J. A. (2014). Cyclone-cyclone interactions through the ocean pathway. *Geophysical Research Letters*, *41*, 6855–6862. https://doi.org/10.1002/2014GL061489

Baranowski, D. B., Flatau, P. J., Chen, S., & Black, P. G. (2014). Upper ocean response to the passage of two sequential typhoons. *Ocean Science*, *10*, 559–570. https://doi.org/10.5194/os-10-559-2014

Black, P. G., D'Asaro, E. A., Drennan, W. M., French, J. R., Niiler, P. P., Sanford, T. B., et al. (2007). Air–sea exchange in hurricanes: Synthesis of observations from the Coupled Boundary Layer Air–Sea Transfer Experiment. *Bulletin of the American Meteorological Society*, *88*, 357–374. https://doi.org/10.1175/BAMS-88-3-357

Brand, S. (1971). The effects on a tropical cyclone of cooler surface waters due to upwelling and mixing produced by a prior tropical cyclone. *Journal of Applied Meteorology*, *10*(5), 865–874.

Bushnell, J. M., & Falvey, R. J. (2017). Annual tropical cyclone report: Joint Typhoon Warning Center.

Chan, J. C. L., Duan, Y., & Shay, L. K. (2001). Tropical cyclone intensity change from a simple ocean-atmosphere coupled model. *Journal of the Atmospheric Sciences*, *58*, 154–172.

Chang, Y.-C., Tseng, R.-S., Chu, P. C., Chen, J.-M., & Centurioni, L. R. (2016). Observed strong currents under global tropical cyclones. *Journal of Marine Systems*, *159*, 33–40. https://doi.org/10.1016/j.jmarsys.2016.03.001

Chen, S., Cummings, J. A., Schmidt, J. M., Sanabia, E. R., & Jayne, S. R. (2017). Targeted ocean sampling guidance for tropical cyclones. *Journal of Geophysical Research: Oceans*, *122*, 3505–3518. https://doi.org/10.1002/2017JC012727

Chen, S., Elsberry, R. L., & Harr, P. A. (2017). Modeling interaction of a tropical cyclone with its cold wake. *Journal of the Atmospheric Sciences*, *74*, 3981–4001. https://doi.org/10.1175/JAS-D-16-0246.1

Chen, Y., Zhang, F., Green, B. W., & Yu, X. (2018). Impacts of ocean cooling and reduced wind drag on Hurricane Katrina (2005) based on numerical simulations. *Monthly Weather Review*, *146*(1), 287–306. https://doi.org/10.1175/MWR-D-17-0170.1

Cione, J. J., & Uhlhorn, E. W. (2003). Sea surface temperature variability in hurricanes: Implications with respect to intensity change. *Monthly Weather Review*, *131*(8), 1783–1796. https://doi.org/10.1175//2562.1

D'Asaro, E. A., Black, P. G., Centurioni, L. R., Chang, Y.-T., Chen, S. S., Foster, R. C., et al. (2014). Impact of typhoons on the ocean in the Pacific. *Bulletin of the American Meteorological Society*, *95*(9), 405–418. https://doi.org/10.1175/BAMS-D-12-00104.1

D'Asaro, E. A., Sanford, T. B., Niiler, P. P., & Terrill, E. J. (2007). Cold wake of Hurricane Frances. *Geophysical Research Letters*, *34*, L15609. https://doi.org/10.1029/2007GL030160

Davis, R. E., Sherman, J. T., & Dufour, J. (2001). Profiling ALACEs and other advances in autonomous subsurface floats. *Journal of Atmospheric and Oceanic Technology*, *18*(6), 982–993. https://doi.org/10.1175/1520-0426(2001)018<0982:PAAOAI>2.0.CO;2

Dee, D. P., Uppala, S. M., Simmons, A. J., Berrisford, P., Poli, P., Kobayashi, S., et al. (2011). The ERA-Interim reanalysis: Configuration and performance of the data assimilation system. *Quarterly Journal of the Royal Meteorological Society*, *137*(656), 553–597. https://doi.org/10.1002/qj.828

Domingues, R., Kuwano-Yoshida, A., Chardon-Maldonado, P., Todd, R. E., Halliwell, G., Kim, H.-S., et al. (2019). Ocean observations in support of studies and forecasts of tropical and extratropical cyclones. *Frontiers in Marine Science*, *6*, 446. https://doi.org/10.3389/fmars.2019.00446

Donlon, C., Robinson, I., Casey, K. S., Vazquez-Cuervo, J., Armstrong, E., Arino, O., et al. (2007). The global ocean data assimilation experiment high-resolution sea surface temperature pilot project. *Bulletin of the American Meteorological Society*, *88*(8), 1197–1214. https://doi.org/10.1175/BAMS-88-8-1197

Emanuel, K. (2003). Tropical cyclones. *Annual Review of Earth and Planetary Sciences*, *31*, 75–104. https://doi.org/10.1146/annurev.earth.31.100901.141259

Goni, G. J., Todd, R. E., Jayne, S. R., Halliwell, G., Glenn, S., Dong, J., et al. (2017). Autonomous and Lagrangian ocean observations for Atlantic tropical cyclone studies and forecasts. *Oceanography*, *30*(2), 92–103. https://doi.org/10.5670/oceanog.2017.227

Hart, R. E., Maue, R. N., & Watson, M. C. (2007). Estimating local memory of tropical cyclones through MPI anomaly evolution. *Monthly Weather Review*, *135*, 3990–4005. https://doi.org/10.1175/2007MWR2038.1

Jayne, S. R., & Bogue, N. M. (2017). Air-deployable profiling floats. *Oceanography*, *30*(2), 29–31. https://doi.org/10.5670/oceanog.2017.214

Johnston, T. M. S., & Rudnick, D. L. (2009). Observations of the transition layer. *Journal of Physical Oceanography*, *39*, 780–797.

Joint Typhoon Warning Center (2018). Prognostic reasoning for STY 26W (Mangkhut) warning NR 19. https://www.webcitation.org/72NwVCj8k

Kitamoto, A. (2017). Digital Typhoon and open science—A trans-disciplinary platform for typhoon-related data. Abstracts of Japan Geoscience Union Meeting 2017.

Knapp, K. R., & Kruk, M. C. (2010). Quantifying interagency differences in tropical cyclone best-track wind speed estimates. *Monthly Weather Review*, *138*, 1459–1473. https://doi.org/10.1175/2009MWR3123.1

Lee, W., Kim, S.-H., Chu, P.-S., Moon, I.-J., & Soloviev, A. V. (2019). An index to better estimate tropical cyclone intensity change in the western North Pacific. *Geophysical Research Letters*, *46*, 8960–8968. https://doi.org/10.1029/2019GL083273

Lin, I-I., Wu, C.-C., Emanuel, K. A., Lee, I.-H., Wu, C.-R., & Pun, I.-F. (2005). The interaction of Supertyphoon Maemi (2003) with a warm ocean eddy. *Monthly Weather Review*, *133*(9), 2635–2649. https://doi.org/10.1175/MWR3005.1

Lin, I.-I., Wu, C.-C., & Pun, I.-F. (2008). Upper-ocean thermal structure and the western North Pacific category 5 typhoons. Part I: Ocean features and the category 5 typhoons' intensification. *Monthly Weather Review*, *136*, 3288–3306. https://doi.org/10.1175/2008MWR2277.1

Lin, S., Zhang, W.-Z., Shang, S.-P., & Hong, H.-S. (2017). Ocean response to typhoons in the western North Pacific: Composite results from Argo data. *Deep Sea Research I*, *123*, 62–74. https://doi.org/10.1016/j.dsr.2017.03.007

Mei, W., Lien, C.-C., Lin, I.-I., & Xie, S.-P. (2015). Tropical cyclone-induced ocean response: A comparative study of the South China Sea and tropical northwest Pacific. *Journal of Climate*, *28*(15), 5952–5968. https://doi.org/10.1175/JCLI-D-14-00651.1

Mitarai, S., & McWilliams, J. C. (2016). Wave glider observations of surface winds and currents in the core of Typhoon Danas. *Geophysical Research Letters*, *43*, 11,312–11,319. https://doi.org/10.1002/2016GL071115

Mitchell, D. A., Teague, W. J., Jarosz, E., & Wang, D. W. (2005). Observed currents over the outer continental shelf during Hurricane Ivan. *Geophysical Research Letters*, *32*, L11610. https://doi.org/10.1029/2005GL023014

Mrvaljevic, R. K., Black, P. G., Centurioni, L. R., Chang, Y.-T., D'Asaro, E. A., Jayne, S. R., et al. (2013). Observations of the cold wake of Typhoon Fanapi (2010). *Geophysical Research Letters*, *40*, 316–321. https://doi.org/10.1029/2012GL054282

Pallàs-Sanz, E., Candela, J., Sheinbaum, J., & Ochoa, J. (2016). Mooring observations of the near-inertial wave wake of Hurricane Ida (2009). *Dynamics of Atmospheres and Oceans*, *76*, 325–344. https://doi.org/10.1016/j.dynatmoce.2016.05.003

Park, J. J., Kwon, Y.-O., & Price, J. F. (2011). Argo array observation of ocean heat content changes induced by tropical cyclones in the north Pacific. *Journal of Geophysical Research*, *116*, C12025. https://doi.org/10.1029/2011JC007165

Price, J. F. (1981). Upper ocean response to a hurricane. *Journal of Physical Oceanography*, *11*, 153–175.

Price, J. F. (2009). Metrics of hurricane-ocean interaction: Vertically-integrated or vertically-averaged ocean temperature? *Ocean Science*, *5*, 351–368. https://doi.org/10.5194/os-5-351-2009

Price, J. F., Morzel, J., & Niiler, P. P. (2008). Warming of SST in the cool wake of a moving hurricane. *Journal of Geophysical Research*, *113*, C07010. https://doi.org/10.1029/2007JC004393

Sanford, T. B., Price, J. F., & Girton, J. B. (2011). Upper-ocean response to Hurricane Frances (2004) observed by profiling EM-APEX floats. *Journal of Physical Oceanography*, *41*, 1041–1056. https://doi.org/10.1175/2010JPO4313.1

Song, J., & Klotzbach, P. J. (2016). Wind structure discrepancies between two best track datasets for western North Pacific tropical cyclones. *Monthly Weather Review*, *144*, 4533–4551. https://doi.org/10.1175/MWR-D-16-0163.1

Sprintall, J., & Tomczak, M. (1992). Evidence of the barrier layer in the surface layer of the tropics. *Journal of Geophysical Research*, *97*(C5), 7305–7316.

Todd, R. E., Asher, T. G., Heiderich, J., Bane, J. M., & Luettich, R. A. (2018). Transient response of the Gulf Stream to multiple hurricanes in 2017. *Geophysical Research Letters*, *45*, 10,509–10,519. https://doi.org/10.1029/2018GL079180

Vincent, E. M., Lengaigne, M., Vialard, J., Madec, G., Jourdain, N. C., & Masson, S. (2012). Assessing the oceanic control on the amplitude of sea surface cooling induced by tropical cyclones. *Journal of Geophysical Research*, *117*, C05023. https://doi.org/10.1029/2011JC007705

Wada, A., Uehara, T., & Ishizaki, S. (2014). Typhoon-induced sea surface cooling during the 2011 and 2012 typhoon seasons: Observational evidence and numerical investigations of the sea surface cooling effect using typhoon simulations. *Search Results Web results Progress in Earth and Planetary Science*, *1*, 11.

Wang, Y., & Wu, C.-C. (2004). Current understanding of tropical cyclone structure and intensity changes—A review. *Meteorology and Atmospheric Physics*, *87*(4), 257–278. https://doi.org/10.1007/s00703-003-0055-6

Wentz, F. J., Gentemann, C., Smith, D., & Chelton, D. (2000). Satellite measurements of sea surface temperature through clouds. *Science*, *288*, 847–850. https://doi.org/10.1126/science.288.5467.847

Wu, C.-C., Lee, C.-Y., & Lin, I-I. (2007). The effect of the ocean eddy on tropical cyclone intensity. *Journal of the Atmospheric Sciences*, *64*(10), 3562–3578. https://doi.org/10.1175/JAS4051.1

Wu, C.-C., Tu, W.-T., Pun, I.-F., Lin, I-I., & Peng, M. S. (2016). Tropical cyclone-ocean interaction in Typhoon Megi (2010)—A synergy study based on ITOP observations and atmosphere-ocean coupled model simulations. *Journal of Geophysical Research: Atmospheres*, *121*, 153–167. https://doi.org/10.1002/2015JD024198

Yu, L., & Weller, R. A. (2007). Objectively analyzed air-sea heat fluxes for the global ice-free oceans (1981–2005). *Bulletin of the American Meteorological Society*, *88*, 527–539. https://doi.org/10.1175/BAMS-88-4-527

Zhang, F., & Emanuel, K. (2018). Promises in air-sea fully coupled data assimilation for future hurricane prediction. *Geophysical Research Letters*, *45*, 13,173–13,177. https://doi.org/10.1029/2018GL080970